Probabilistic Approach to Detect and Correct GNSS NLOS Signals Using an Augmented State Vector in the Extended Kalman Filter

Changhui Jiang[1], Bing Xu[1]* and Li-Ta Hsu[1]

1. Interdisciplinary Division of Aeronautical and Aviation Engineering, The Hong Kong Polytechnic University, Hong Kong

Abstract Non-line-of-sight (NLOS) global navigation satellite system (GNSS) signals are a major factor that limits the GNSS positioning accuracy in urban areas. An advanced GNSS signal processing technique, the vector tracking loop (VTL), has been applied to NLOS detection and correction, and its feasibility and superior performance have been reported in recent studies. In a VTL-based GNSS receiver, the navigation (i.e., position, velocity and time (PVT)) solutions are used to predict the signal tracking loop parameters. The difference between the predicted signal and the received signal within the code discriminator output can be used to detect NLOS reception. We generate the probability of NLOS detection by modelling the code discriminator outputs using Gaussian fitting. If this probability is larger than a predefined threshold, NLOS reception is deemed to occur. Then, the NLOS-induced pseudorange measurement bias is estimated as a state variable in the state vector; i.e., an augmented state vector is created for the extended Kalman filter. Two GPS L1 C/A signal datasets from a static test and a dynamic test are investigated using the proposed algorithm. The experimental results indicate that when NLOS reception is present, the proposed approach outperforms the other two methods, i.e., the standard VTL method without considering NLOS reception and the VTL-based NLOS detection and correction method with multicorrelators, in terms of the positioning performance. In addition, the proposed approach has a lower computational load than the VTL method with multicorrelators.

Keywords: GNSS, NLOS, Vector Tracking Loop, Gaussian Fitting, Augmented state

vector, Kalman Filter

* Correspondence: Bing Xu (E-mail: pbing.xu@polyu.edu.hk)

Introduction

Urban areas characterized by tall buildings and narrow streets are challenging for global navigation satellite system (GNSS) positioning. To deliver user position, velocity and time (PVT) information, one synchronizes GNSS signals to local signal replicas within the receiver to generate measurements such as pseudorange measurements, carrier Doppler frequencies, and the carrier-to-noise power ratio C/N_0. Under an open-sky environment, the received signals almost all directly reach the receiver antenna (Kaplan and Hegarty 2005; Tsui 2005). As such, accurate synchronization is achievable, and therefore, accurate navigation solutions can be obtained. However, in dense urban areas, the signals are easily reflected or blocked by tall buildings, leading to multipath (MP) interference and non-line-of-sight (NLOS) reception. MP signals refer to compound signals with both direct and reflected signals or multiple reflected signals with no direct signals, whereas an NLOS signal contains only the time-delayed version of the direct signal (Hsu 2018). MP interference and NLOS signals can degrade the measurement quality and cause large positioning errors. In particular, the NLOS-induced pseudorange measurement error could reach tens of metres. As such, in this work, we focus on the issue of NLOS signals, although the proposed algorithm could be extended to MP-induced error detection and correction.

Researchers have proposed various methods of dealing with NLOS signals to improve the accuracy of standalone GNSS receivers (Breßler et al. 2016). These techniques and algorithms can be broadly divided into two categories: detection and correction. Detection algorithms are the premise for mitigating or correcting NLOS signals. In general, an NLOS signal has a lower C/N_0 than a direct line-of-sight (LOS) signal, and thus, this power ratio can be used as a detection metric. Apart from C/N_0, other features of NLOS signals are also explored in the literature using machine learning techniques at both the Receiver Independent Exchange Format (RINEX) level and the baseband signal processing level (Xu et al. 2019b; Yozevitch et al. 2016). In addition, external assistance, such as 3D building models (Wang et al. 2015; Hsu et al. 2015a) and a sky-pointing camera, can also be employed for detecting NLOS reception (Meguro et al. 2009; Marais et al. 2014).

In dense urban areas, in-view satellites usually have a poor geometric distribution due to blockage. As such, an ideal method is to constructively use NLOS signals instead of excluding them to avoid degrading the satellite geometry. The NLOS signal time delay can be estimated with additional assistance, e.g., a 3D building model, with which the signal propagation route can be traced using the ray tracing technique, and therefore, the additional time delay can be obtained. However, the ray tracing method may take approximately half a minute to one minute to propagate the transmission paths for all satellites to all surfaces inside the 3D model; the required computation time depends on the complexity of the 3D building model (Ng et al. 2020). To avoid requiring assistance from external sensors, such as inertial measurement units, cameras, 2D/3D mapping, or other forms, the advanced GNSS signal processing technique known as the vector tracking loop (VTL) has been proposed to detect and correct NLOS reception in recent years (Hsu et al. 2015b; Xu et al. 2020).

The concept of the VTL dates back to the early 1980s (Copps et al. 1980). In the VTL technique, signal tracking and navigation processing are considered a single integrated function, not separate functions. Spilker (1996) described the structure of the vector delay lock loop (VDLL), which laid the foundation for wide applications of VTL. The most cited benefit of the VTL over conventional scalar tracking loops (STLs) is its robustness in challenging environments, e.g., weak signals and high dynamics (Lashley et al. 2009; Zhao et al. 2011), signal outages (Jiang et al. 2019), and interference (Benson 2007). In terms of dealing with the NLOS issue, VTL has also been explored in the existing literature. In Hsu et al. (2015b), NLOS detection was accomplished using VTL. The rationale behind this approach is that the VTL closes the tracking loop using the navigation solutions. In this way, the NLOS signal is not locked onto given an accurate navigation solution using other healthy satellites and a receiver dynamics model. Therefore, a phase difference between the incoming NLOS signal and the local replica code is created and remains during the NLOS reception period, which provides an opportunity for detecting NLOS reception. Recently, Xu et al. (2020) developed a robust and comprehensive algorithm based on an open-source VTL software-defined receiver (SDR) (Xu and Hsu 2019a) that can not only detect NLOS reception but also correct NLOS-induced pseudorange measurement errors. However, this algorithm detects NLOS signals using the time delays of multicorrelator peaks and therefore suffers from a high computational load. To address this issue, Xu et al developed a two-step algorithm. In the first step, a potential NLOS subset is determined by a metric, the noise bandwidth, based on the fact that the VTL adaptively gives a lower noise bandwidth to contaminated signals, including received NLOS signals. In the second step, multicorrelators are activated in channels for potential NLOS reception to claim and extract the NLOS code delay. However, the noise bandwidth is related to specifications on the front end, such as the filter bandwidth and the noise level. In addition, a premise of this method is that four or more healthy satellites exist; otherwise, the accuracy of the navigation solution will degrade, and thus, the algorithm can no longer provide accurate loop parameters, as demonstrated in Fig. 26 in Xu et al. (2020). Therefore, it is difficult for this algorithm to cope with more complicated environments, e.g., a large portion of contaminated measurements. Therefore, there is still much room for improving the VTL-based NLOS detection and correction approach. For instance, how does one effectively detect and correct NLOS reception without using multicorrelators? Another question is how to enhance the robustness against complicated environments.

In the VTL framework, an extended Kalman filter (EKF) is usually employed for estimating the user position and clock bias based on the VDLL discriminator outputs. Under the LOS condition, the error of the VDLL discriminator outputs is assumed to be subject to a zero-mean Gaussian distribution. However, when NLOS signals are received, the statistics of the VDLL discriminator outputs will change. To cope with this problem, we augment the standard state vector, which consists of user position and velocity errors and user clock bias and drift errors, with an extra term, i.e., the NLOS-induced code delay. Consequently, an EKF with an augmented state is designed to estimate the NLOS-induced pseudorange measurement error along with the navigation solutions. In fact, the probability of NLOS occurrence can also be inferred from the statistics of code discriminator outputs. As such, NLOS occurrence can be detected with the constructed statistical model. In summary, we propose an approach to detect and correct GNSS NLOS-induced errors by augmenting the state vector with NLOS-induced biases for estimation with an EKF. Compared with the existing literature, our contributions are summarized as follows:

(1) A Gaussian fitting (GF) method is proposed to model the VDLL discriminator outputs, and the probability of NLOS detection can be generated. Once the NLOS occurrence detection probability is larger than the predefined threshold, the NLOS signal is deemed present. Detection and false alarm curves are also presented for analysing the proposed detection method.

(2) In the existing method (Xu et al. 2020), the NLOS bias is estimated using the average values of multicorrelator outputs, and the measurements are compensated with the average values of the code discriminator outputs before being included in the navigation solution determination process. We add the NLOS-induced bias to the state vector for estimation in the EKF. In this way, a more accurate NLOS bias can be estimated, leading to an improved PVT solution.

The following section describes the methodology, including the designed VTL navigation filters under LOS and NLOS conditions and the NLOS probabilistic detection algorithm. This is followed by the experimental section, in which we test two GPS L1 C/A signal datasets. Detailed results and an in-depth analysis are presented. Finally, we conclude the paper and provide suggestions for future work.

Methodology

In this section, we introduce the proposed methodology. Fig. 1 illustrates a system-level block diagram of the proposed method. The probability of NLOS detection at each channel is calculated based on the VDLL discriminator outputs. If the NLOS detection probability is larger than a threshold, the corresponding NLOS bias will be added to the state vector to be estimated. If NLOS signals are not present, the commonly used state vector will be used in the EKF.

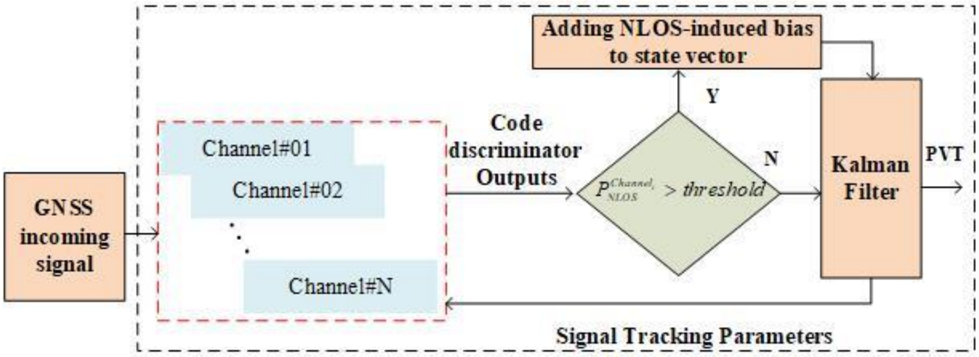

Fig. 1 System-level block diagram of the proposed method.

VTL Navigation Filter under LOS Condition

In the standard VTL navigation filter model, the error state vector, $\delta\mathbf{x}$, is usually defined as (Zhao et al. 2011):

$$\delta\mathbf{x} = [\delta\mathbf{p}, \delta\mathbf{v}, \delta t_b, \delta t_d]^{\mathrm{T}} \tag{1}$$

where $\delta\mathbf{p}$ and $\delta\mathbf{v}$ are error vectors of the user position and velocity, respectively, in Earth centred Earth fixed (ECEF) coordinates, δt_b is the user clock bias error in metres, and δt_d is the user clock drift error in units of metres per second. The system propagation equation is

$$\delta\mathbf{x}_{k+1} = \mathbf{\Phi}^{\mathrm{LOS}}\delta\mathbf{x}_k + \mathbf{w}_k \tag{2}$$

where $\mathbf{w}_{k+1}$ is the process noise vector with an assumed zero mean and normal distribution, i.e., $\mathbf{w}_k \sim \mathcal{N}\left(0, \mathbf{Q}_k\right)$ with covariance matrix $\mathbf{Q}_k$, and $\mathbf{\Phi}^{\mathrm{LOS}}$ is the state transition matrix, which is assumed to be

$$\mathbf{\Phi}^{\mathrm{LOS}} = \begin{bmatrix} \mathbf{I}_{3\times3} & T_0\mathbf{I}_{3\times3} & \mathbf{0}_{3\times2} \\ \mathbf{0}_{3\times3} & \mathbf{I}_{3\times3} & \mathbf{0}_{3\times2} \\ \mathbf{0}_{2\times3} & \mathbf{0}_{2\times3} & \begin{bmatrix} 1 & T_0 \\ 0 & 1 \end{bmatrix} \end{bmatrix} \tag{3}$$

with T_0 being the update interval. The superscript "LOS" denotes the LOS condition.

In the VTL, carrier tracking is accomplished via a vector frequency lock loop (VFLL). The user velocity error vector at $k+1$, $\delta\mathbf{v}_{k+1}^{\mathrm{T}}$, can be inferred from the pseudorange rate error measurements $\delta\mathbf{z}_{k+1}^{\mathrm{ca}}$ using

$$\delta\mathbf{z}_{k+1}^{\mathrm{ca}} = \mathbf{H}_{k+1}^{\mathrm{ca}}\delta\mathbf{v}_{k+1}^{\mathrm{T}} + \begin{bmatrix}1 & 1 & \cdots & 1\end{bmatrix}_{1\times M}^{\mathrm{T}} \delta t_{d,k+1} + \boldsymbol{\varepsilon}_{k+1}^{\mathrm{ca}} \tag{4}$$

where $\mathbf{H}_{k+1}^{ca} = \begin{bmatrix} -l_x^{(1)} & -l_y^{(1)} & -l_z^{(1)} \\ -l_x^{(2)} & -l_y^{(2)} & -l_z^{(2)} \\ \vdots & \vdots & \vdots \\ -l_x^{(M)} & -l_y^{(M)} & -l_z^{(M)} \end{bmatrix}$, $\begin{bmatrix}-l_x^{(m)} & -l_y^{(m)} & -l_z^{(m)}\end{bmatrix} = \left(\mathbf{p}^{(m)} - \mathbf{p}_u\right) / \left\|\mathbf{p}^{(m)} - \mathbf{p}_u\right\|$ is the unit vector pointing from the receiver to the *m*-th satellite, and $\mathbf{p}^{(m)}$ and $\mathbf{p}_u$ are the position vectors of the *m*-th satellite and receiver, respectively. $\delta t_{d,k+1}$ represents the receiver clock drift error. $\boldsymbol{\varepsilon}_k^{\mathrm{ca}}$ denotes the measurement noise vector for the pseudorange rate error measurement. The code discriminator outputs are employed as the pseudorange error measurements, $\delta\mathbf{z}_{k+1}^{\mathrm{c}}$, which are related to the state variable as

$$\delta\mathbf{z}_{k+1}^{\mathrm{c}} = \mathbf{H}_{k+1}^{\mathrm{c}} \cdot \delta\mathbf{p}_{k+1}^{\mathrm{T}} + \begin{bmatrix}1 & 1 & \cdots & 1\end{bmatrix}_{1\times M}^{\mathrm{T}} \cdot \delta t_{b,k+1} + \boldsymbol{\varepsilon}_{k+1}^{\mathrm{c}} \tag{5}$$

where $\mathbf{H}_{k+1}^{\mathrm{c}} = \mathbf{H}_{k+1}^{\mathrm{ca}}$ and $\boldsymbol{\varepsilon}_{k+1}^{\mathrm{c}}$ is the measurement noise vector for the pseudorange error measurement.

Equations (1) to (5) illustrate the relationship between the state variables and the measurement variables. The Kalman filter works as a two-step process. In the first step, i.e., prediction, the filter predicts the state at the next epoch along with its uncertainty $\mathbf{P}_{k+1}$, which is referred to as the state estimation error covariance matrix, using

$$\delta \mathbf{x}_{k+1}^{-} = \mathbf{\Phi}^{\mathrm{LOS}} \cdot \delta \mathbf{x}_{k} \tag{6}$$

$$\mathbf{P}_{k+1}^{-} = \mathbf{\Phi}^{\mathrm{LOS}} \mathbf{P}_{k} \left(\mathbf{\Phi}^{\mathrm{LOS}}\right)^{\mathrm{T}} + \mathbf{Q}_{k} \tag{7}$$

where '-' denotes a prediction and $\mathbf{Q}_k = E\left(\mathbf{w}_k \mathbf{w}_k^{\mathrm{T}}\right)$, with $E(\cdot)$ being the expectation operator.

In the second step, the state is updated in a weighted average manner based on the uncertainties in the system propagation and the measurements

$$\delta \mathbf{x}_{k+1} = \delta \mathbf{x}_{k+1}^{-} + \mathbf{K}_{k+1}\left(\delta \mathbf{z}_{k+1} - \mathbf{H}_{k+1}^{\mathrm{LOS}} \delta \mathbf{x}_{k+1}^{-}\right) \tag{8}$$

$$\mathbf{K}_{k+1} = \mathbf{P}_{k+1}^{-} (\mathbf{H}_{k+1}^{\mathrm{LOS}})^{T} \left[\mathbf{H}_{k+1}^{\mathrm{LOS}} \mathbf{P}_{k+1}^{-} \left(\mathbf{H}_{k+1}^{\mathrm{LOS}}\right)^{\mathrm{T}} + \mathbf{R}_{k+1}\right]^{-1} \tag{9}$$

$$\mathbf{P}_{k+1} = \left(\mathbf{I} - \mathbf{K}_{k+1} \mathbf{H}_{k+1}^{\mathrm{LOS}}\right) \mathbf{P}_{k+1}^{-} \tag{10}$$

where $\delta \mathbf{z}_{k+1} = \begin{bmatrix} \delta \mathbf{z}_{k+1}^{\mathrm{c}} \\ \delta \mathbf{z}_{k+1}^{\mathrm{ca}} \end{bmatrix}$, $\mathbf{H}_{k+1}^{\mathrm{LOS}} = \begin{bmatrix} \mathbf{H}_{k+1}^{\mathrm{c}} & \mathbf{0}_{M\times 3} & \mathbf{A} \\ \mathbf{0}_{M\times 3} & \mathbf{H}_{k+1}^{\mathrm{ca}} & \mathbf{B} \end{bmatrix}$, $\mathbf{A} = \begin{bmatrix} 1 & 0 \\ 1 & 0 \\ \vdots & \vdots \\ 1 & 0 \end{bmatrix}_{M\times 2}$, $\mathbf{B} = \begin{bmatrix} 0 & 1 \\ 0 & 1 \\ \vdots & \vdots \\ 0 & 1 \end{bmatrix}_{M\times 2}$,

$\mathbf{K}_{k+1}$ is the Kalman gain matrix, $\mathbf{I}$ is an identity matrix with the same dimensions as $\mathbf{P}_{k+1}$, and $\mathbf{R}_{k+1}$ is the measurement noise covariance matrix that is calculated by $\mathbf{R}_k = E\left(\boldsymbol{\varepsilon}_k \boldsymbol{\varepsilon}_k^{\mathrm{T}}\right)$. The VTL navigation filter works in a recursive manner as described by (6) to (10) under the LOS condition. When NLOS reception is present, the NLOS-induced pseudorange error is added to the state described in (1), forming an augmented state, which is described in the following subsection.

VTL Navigation Filter under the NLOS Condition

As stated previously, the additional time delay of the NLOS signal will distort the VTL navigation filter measurements, leading to erroneous navigation solutions. Therefore, before updating the navigation filter, the NLOS signal should be detected from the received signals. Upon detection, instead of excluding the NLOS signal measurements, we propose to correct the NLOS-induced measurement error to constructively use it without degrading the satellite geometry.

In the existing VTL-based NLOS detection and correction method (Xu et al. 2020), the occurrence of the NLOS signal is determined based on the multicorrelator output, from which the NLOS delay can also be extracted. However, the corresponding computations require a large amount of computational resources, and the resolution is limited by the number of correlators used. In this research, we detect NLOS reception and correct the NLOS-induced measurement error without using multicorrelators. The rationale behind this approach is that the code discriminator outputs are subject to a zero-mean Gaussian distribution under pure LOS conditions and a non-zero-mean Gaussian distribution under the NLOS condition. Note that, to obtain accurate Gaussian model parameters, this approach should be applied when the tracking loop reaches its steady state. When the NLOS signal is present, the measurement model of (5) is modified to

$$\delta \mathbf{z}_{k+1}^{\mathrm{c}} = \mathbf{H}_{k+1}^{\mathrm{c}} \cdot \delta \mathbf{p}_{k+1}^{\mathrm{T}} + \cdot \delta t_{b,k+1} + \mathbf{b}^{\mathrm{NLOS}} + \boldsymbol{\varepsilon}_{k+1}^{\mathrm{c}} \tag{11}$$

where $\mathbf{b}^{\mathrm{NLOS}}$ is the NLOS-induced pseudorange measurement error in units of metres. The superscript “NLOS” denotes the variables under the NLOS condition. By adding $\mathbf{b}^{\mathrm{NLOS}}$ to (1), an augmented state is formed as

$$\delta \mathbf{x}^{\mathrm{NLOS}} = [\delta \mathbf{p}, \delta \mathbf{v}, \delta t_b, \delta t_d, \mathbf{b}^{\mathrm{NLOS}}]^{\mathrm{T}} \tag{12}$$

Note that the dimension of $\mathbf{b}^{\mathrm{NLOS}}$ equals the number of satellites that are identified as providing NLOS signals. With the introduction of $\mathbf{b}^{\mathrm{NLOS}}$, the Kalman filter models are rewritten as

$$\delta \mathbf{x}_{k+1}^{\mathrm{NLOS}} = \mathbf{\Phi}^{\mathrm{NLOS}} \delta \mathbf{x}_{k}^{\mathrm{NLOS}} + \mathbf{w}_{k+1}^{\mathrm{NLOS}} \tag{13}$$

$$\delta \mathbf{z}_{k+1}^{\mathrm{NLOS}} = \mathbf{H}_{k+1}^{\mathrm{NLOS}} \cdot \delta \mathbf{x}_{k+1}^{\mathrm{NLOS}} + \boldsymbol{\varepsilon}_{k+1}^{\mathrm{NLOS}} \tag{14}$$

Considering that LOS and NLOS signals can be present at the same time, (13) and (14) are reformulated as

$$\begin{bmatrix} \delta \mathbf{x}_{k+1}^{\mathrm{LOS}} \\ \mathbf{b}_{k+1}^{\mathrm{NLOS}} \end{bmatrix} = \begin{bmatrix} \boldsymbol{\Phi}^{\mathrm{LOS}} & \mathbf{0} \\ \mathbf{0} & \mathbf{I} \end{bmatrix} \cdot \begin{bmatrix} \mathbf{x}_{k}^{\mathrm{LOS}} \\ \mathbf{b}_{k}^{\mathrm{NLOS}} \end{bmatrix} + \mathbf{w}_{k+1}^{\mathrm{NLOS}} \tag{15}$$

$$\delta \mathbf{z}_{k+1}^{\mathrm{NLOS}} = \mathbf{H}_{k+1}^{\mathrm{NLOS}} \cdot \begin{bmatrix} \delta \mathbf{x}_{k+1}^{\mathrm{LOS}} \\ \mathbf{b}_{k+1}^{\mathrm{NLOS}} \end{bmatrix} + \boldsymbol{\varepsilon}_{k+1}^{\mathrm{NLOS}} \tag{16}$$

where $\mathbf{H}_{k+1}^{\mathrm{NLOS}} = \begin{bmatrix} \mathbf{H}_{k+1}^{\mathrm{c}} & \mathbf{0}_{M\times 3} & \mathbf{A} & \mathbf{C}_{M\times 1} \\ \mathbf{0}_{M\times 3} & \mathbf{H}_{k+1}^{\mathrm{ca}} & \mathbf{B} & \mathbf{0}_{M\times 1} \end{bmatrix}$ and $\mathbf{C}_{M\times 1}$ is a matrix with entries of 1 and 0 for NLOS and LOS signals, respectively. As a result, the prediction and updating processes of the Kalman filter can be summarized as

$$\begin{bmatrix} \left(\delta \mathbf{x}_{k+1}^{\mathrm{LOS}}\right)^{-} \\ \left(\mathbf{b}_{k+1}^{\mathrm{NLOS}}\right)^{-} \end{bmatrix} = \begin{bmatrix} \boldsymbol{\Phi}^{\mathrm{LOS}} & \mathbf{0} \\ \mathbf{0} & \mathbf{I} \end{bmatrix} \begin{bmatrix} \delta \mathbf{x}_{k}^{\mathrm{LOS}} \\ \mathbf{b}_{k}^{\mathrm{NLOS}} \end{bmatrix} \tag{17}$$

$$\left(\mathbf{P}_{k+1}^{\mathrm{NLOS}}\right)^{-} = \begin{bmatrix} \boldsymbol{\Phi}^{\mathrm{LOS}} & \mathbf{0} \\ \mathbf{0} & \mathbf{I} \end{bmatrix} \begin{bmatrix} \mathbf{P}_{k} & \mathbf{0} \\ \mathbf{0} & \mathbf{B}_{0} \end{bmatrix} \begin{bmatrix} \boldsymbol{\Phi}^{\mathrm{LOS}} & \mathbf{0} \\ \mathbf{0} & \mathbf{I} \end{bmatrix}^{\mathrm{T}} + \mathbf{Q}_{k+1}^{\mathrm{NLOS}} \tag{18}$$

$$\mathbf{K}_{k+1}^{\mathrm{NLOS}} = \left(\mathbf{P}_{k+1}^{\mathrm{NLOS}}\right)^{-} \left[\mathbf{H}^{\mathrm{NLOS}} \right]^{\mathrm{T}} \left(\mathbf{H}^{\mathrm{NLOS}} \left(\mathbf{P}_{k+1}^{\mathrm{NLOS}}\right)^{-} \left[\mathbf{H}^{\mathrm{NLOS}} \right]^{\mathrm{T}} + \mathbf{R}_{k+1}^{\mathrm{NLOS}} \right)^{-1} \tag{19}$$

$$\begin{bmatrix} \delta \mathbf{x}_{k+1}^{\mathrm{LOS}} \\ \mathbf{b}_{k+1}^{\mathrm{NLOS}} \end{bmatrix} = \begin{bmatrix} \left(\delta \mathbf{x}_{k+1}^{\mathrm{LOS}}\right)^{-} \\ \left(\mathbf{b}_{k+1}^{\mathrm{NLOS}}\right)^{-} \end{bmatrix} + \mathbf{K}_{k+1}^{\mathrm{NLOS}} \left(\delta \mathbf{z}_{k}^{\mathrm{NLOS}} - \mathbf{H}^{\mathrm{NLOS}} \begin{bmatrix} \left(\delta \mathbf{x}_{k+1}^{\mathrm{LOS}}\right)^{-} \\ \left(\mathbf{b}_{k+1}^{\mathrm{NLOS}}\right)^{-} \end{bmatrix} \right) \tag{20}$$

$$\mathbf{P}_{k+1}^{\mathrm{NLOS}} = \left(\mathbf{I} - \mathbf{K}_{k+1}^{\mathrm{NLOS}} \left[\mathbf{H}^{\mathrm{NLOS}} \right] \right) \left(\mathbf{P}_{k+1}^{\mathrm{NLOS}} \right)^{-} \tag{21}$$

where $\mathbf{Q}_{k}^{\mathrm{NLOS}} = E\left(\mathbf{w}_{k}^{\mathrm{NLOS}} \left(\mathbf{w}_{k}^{\mathrm{NLOS}}\right)^{\mathrm{T}} \right)$, $\mathbf{R}_{k}^{\mathrm{NLOS}} = E\left(\boldsymbol{\varepsilon}_{k}^{\mathrm{NLOS}} \left(\boldsymbol{\varepsilon}_{i}^{\mathrm{NLOS}}\right)^{\mathrm{T}} \right)$, and $\mathbf{B}_{0}$ is the state estimation error covariance matrix associated with $\mathbf{b}^{\mathrm{NLOS}}$. Compared with (6) through (10), which describe the VTL navigation filter under the LOS condition, the navigation filter under the NLOS condition, i.e., (17) to (21), can estimate the NLOS-induced pseudorange measurement error in addition to the PVT solution.

NLOS Detection

In the existing VTL-based NLOS detection method, NLOS detection is accomplished based on multicorrelator outputs. The bias of the correlator peak, $\Delta\tau$, is assumed to be the additional code delay of the NLOS reception. If $\Delta\tau$ exceeds a predetermined threshold, NLOS reception is deemed present. Here, we use a Gaussian model to fit the code discriminator outputs and generate the probability of LOS/NLOS occurrence. Additionally, with the given parameters, the false detection probability and false alarm probability of NLOS reception can be generated.

The VDLL discriminator outputs are assumed to be subject to a Gaussian distribution. As such, the *i*-th epoch code discriminator output CE_i can be modelled as

$$CE_i \sim \mathcal{N}\left(u_{CE_i}, \sigma_{CE_i}^2\right) \tag{22}$$

where $\mathcal{N}(\cdot)$ denotes the normal distribution, u_{CE_i} and $\sigma_{CE_i}^2$ are the expectation and variance, respectively, of the *i*-th epoch code discriminator output. Under the LOS condition, $u_{CE_i} = 0$. The average values $Avg\_CE_i = \sum_{k=i}^{N_{CE}+i-1} CE_k \Big/ N_{CE}$, where N_{CE} is the number of code discriminator outputs being calculated, are still subject to a Gaussian distribution and thus is modelled using

$$Avg\_CE_i \sim \mathcal{N}\left(\frac{\sum_{k=i}^{N_{CE}+i-1} u_{CE_k}}{N_{CE}}, \frac{\sum_{k=i}^{N_{CE}+i-1} \sigma_{CE_k}^2}{N_{CE}^2}\right) \tag{23}$$

under the assumption that CE_i is independently distributed. Assuming that H_0 represents LOS occurrence and H_1 represents NLOS occurrence, the NLOS detection probability P_d is

$$P_d = P\left(Avg\_CE_i > \alpha \mid H_1\right) = 1 - P\left(Avg\_CE_i < \alpha \mid H_1\right) \tag{24}$$

where α is the NLOS detection threshold and $P(\cdot)$ is the cumulative distribution function. In fact, Avg_CE_i is not necessarily subject to a normal Gaussian distribution. To calculate the detection probability, we transform the Gaussian distribution in a normalized Gaussian distribution as follows

$$\left(\frac{Avg\_CE_i - \frac{\sum_{k=i}^{N_{CE}+i-1} u_{CE_k}}{N_{CE}}}{\sqrt{\frac{\sum_{k=i}^{N_{CE}+i-1} \sigma_{CE_k}^2}{N_{CE}^2}}}\right) \sim \mathcal{N}(0,1) \tag{25}$$

$$P_d = P\left(\frac{Avg\_CE_i - \frac{\sum_{k=i}^{N_{CE}+i-1} u_{CE_k}}{N_{CE}}}{\sqrt{\frac{\sum_{k=i}^{N_{CE}+i-1} \sigma_{CE_k}^2}{N_{CE}^2}}} < \frac{\alpha - \frac{\sum_{k=i}^{N_{CE}+i-1} u_{CE_k}}{N_{CE}}}{\sqrt{\frac{\sum_{k=i}^{N_{CE}+i-1} \sigma_{CE_k}^2}{N_{CE}^2}}} \mid H_1\right) \tag{26}$$

where the detection probability is established as a function of Avg_CE_i, the detection threshold and the statistical parameters in the Gaussian distribution framework. The NLOS probability corresponding to each Avg_CE_i can be calculated with this established model. Under the LOS condition, the distribution of Avg_CE_i is described as

$$Avg\_CE_i \sim \mathcal{N}\left(0, \frac{\sum_{k=i}^{N_{CE}+i-1} \sigma_{CE_k}^2}{N_{CE}^2}\right) \tag{27}$$

where Avg_CE_i is assumed to be subject to a zero-mean Gaussian distribution. In this context, a false alarm refers to the case when an NLOS signal is detected but is in fact an LOS signal. The false alarm probability P_{fa} is

$$P_{fa} = P\left(Avg\_CE_i > \alpha \mid H_0\right) = 1 - P\left(Avg\_CE_i < \alpha \mid H_0\right) \tag{28}$$

where P_{fa} is calculated based on the LOS occurrence probability, $P\left(Avg\_CE_i < \alpha \mid H_0\right)$. Similar to (24) to (26), the transformation of the distribution of Avg_CE_i to a normalized Gaussian distribution and the calculation of the false alarm probability is given by

$$\frac{Avg\_CE_i}{\sqrt{\frac{\sum_{k=i}^{N_{CE}+i-1} \sigma_{CE_k}^2}{N_{CE}^2}}} \sim \mathcal{N}\left(0,1\right) \tag{29}$$

$$P_{fa} = 1 - P\left(\frac{Avg\_CE}{\sqrt{\frac{\sum_{k=i}^{N_{CE}+i-1} \sigma_{CE_k}^2}{N_{CE}^2}}} < \frac{\alpha}{\sqrt{\frac{\sum_{k=i}^{N_{CE}+i-1} \sigma_{CE_k}^2}{N_{CE}^2}}} \mid H_0 \right) \tag{30}$$

As seen in (30), the false alarm probability is also related to the detection threshold α. In fact, a smaller false alarm probability is always preferred in detection. The relationship between the NLOS detection probability and the false alarm probability can be established through the shared detection threshold.

According to (30), the NLOS detection threshold α can be written as

$$\alpha = P^{-1}\left(1 - P_{fa}\right) \cdot \sqrt{\frac{\sum_{k=i}^{N_{CE}+i-1} \sigma_{CE_k}^2}{N_{CE}^2}} \tag{31}$$

where $P^{-1}\left(\cdot\right)$ is the inverse distribution function of the standard Gaussian distribution. Combining (26) and (31), the relationship between detection probability P_d and false alarm probability P_{fa} is written as

$$P_d = 1 - P\left(\frac{P^{-1}\left(1-P_{fa}\right)\cdot\sqrt{\frac{\sum_{k=i}^{N_{CE}+i-1}\sigma_{CE_k}^2}{N_{CE}^2}} - \frac{\sum_{k=i}^{N_{CE}+i-1}u_{CE_k}}{N_{CE}}}{\sqrt{\frac{\sum_{k=i}^{N_{CE}+i-1}\sigma_{CE_k}^2}{N_{CE}^2}}} \right) \tag{32}$$

where the NLOS detection probability P_d is modelled as a function of the false alarm probability P_{fa} and the statistical parameters u_{CE_k} and σ_{CE_k}. Letting $u_{CE_k}=\sigma$ and $\mu_{CE_k}=\mu$, equation (32) can be simplified to

$$\begin{aligned} P_d &= 1 - P\left(P^{-1}\left(1-P_{fa}\right) - \frac{\mu}{\sigma}\cdot\sqrt{N_{CE}} \right) \\ &= 1 - P\left(P^{-1}\left(1-P_{fa}\right) - \beta\cdot\sqrt{N_{CE}} \right) \end{aligned} \tag{33}$$

where $\frac{\mu}{\sigma}=\beta$. As can be seen, the parameters β and N_{CE} affect the relationship between the NLOS detection probability P_d and the false alarm probability P_{fa}. N_{CE} can be either selected as a rule-of-thumb value or determined by analysing the relationship between P_d and P_{fa} in (33). While implementing the method, the parameters N_{CE}, u_{CE_k} and σ_{CE_k} are usually set through an experimental analysis of the code discriminator outputs.

Experiments

In this section, both static and dynamic field tests are carried out to evaluate the performance of the proposed algorithm using GPS L1 C/A signals. We present detailed results such as the LOS/NLOS detection probability, the relationship between the false alarm probability and detection probability, and the positioning performance.

Static Field Test

A static field test was conducted at an irregular crossroad in the Tsim Sha Tsui East area, Hong Kong, as shown in Fig. 2, together with a sky plot of the building boundary information during the test period. Table 1 lists the parameter settings of the data collection equipment. As shown in Fig. 2, seven satellites are tracked, among which pseudorandom noise (PRN) 3 and 22 are NLOS satellites. Fig. 3 shows the signal strength of the satellites. PRNs 3 and 22 have lower powers than the other satellites due to reflection-induced attenuation.

Table 1 Parameter settings of the data collection equipment

Equipment	Parameter	Value	Unit
Antenna	Model	AGR6303	-
	Low noise amplifier gain	27	dB
	Noise figure	≤ 2	dB
	Polarization	Right-hand circularly polarized	-
Front-end	Model	NSL Stereo	-
	GNSS signal	GPS L1 C/A	-
	Sampling frequency	26	MHz
	Intermediate frequency	0	MHz
	Double-sided bandwidth	8	MHz
	Noise figure	8	dB
	Gain	10	dB

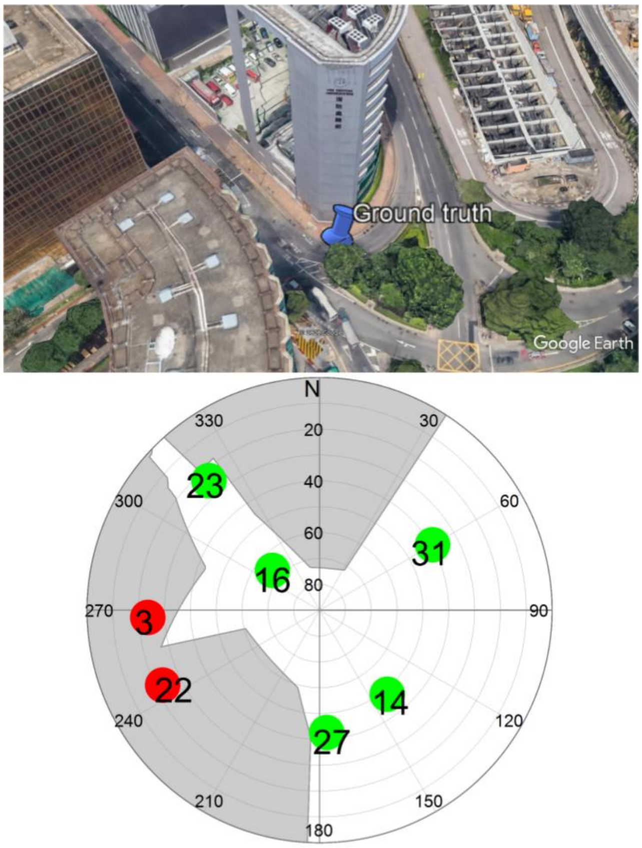

Fig. 2 Static experimental point in Google Earth (top) and a sky plot with building boundary information (bottom, Green: LOS, Red: NLOS; numbers indicate the PRN index)

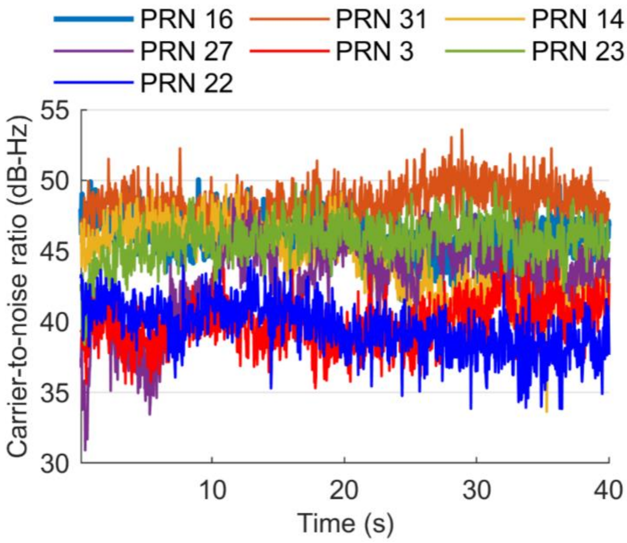

Fig. 3 Signal C/N_0 of the satellites tracked

We model the VDLL discriminator outputs using GF (Chen et al. 2018) and extract the statistical parameters for calculating the NLOS occurrence detection probability and the corresponding false alarm probability. Figs. 4 and 5 present the GF results of the VDLL discriminator outputs for LOS satellites (PRNs 14, 16, 23, 27, and 31) and NLOS satellites (PRNs 3 and 22), respectively. The GF results are obtained using the first 40 seconds of data. The coherent integration time is set to 1 millisecond (ms), and 40000 code discriminator outputs are used here. It is observed that the LOS and NLOS signals are distinguishable in terms of the mean value of the GF-fitted VDLL discriminator outputs, and this characteristic is helpful for detecting NLOS occurrence. For this dataset, the mean value of the discriminator outputs for the LOS signals approaches zero, whereas the mean value has a larger offset (≤ -0.2 chip) for the NLOS signals. Note that the mean value of the code discriminator outputs can be either positive or negative for LOS and MP signals, whereas the mean value is negative for NLOS satellites. The reason is that an NLOS signal travels along an additional path and therefore aligns better with the late correlator than the early correlator in the VTL architecture. As a result, for an early minus late discriminator function, its output is negative. However, for MP signals, the code discriminator output can be either positively or negatively dependent on the carrier phase difference between the direct signal and the reflected signal (Xu et al. 2019b).

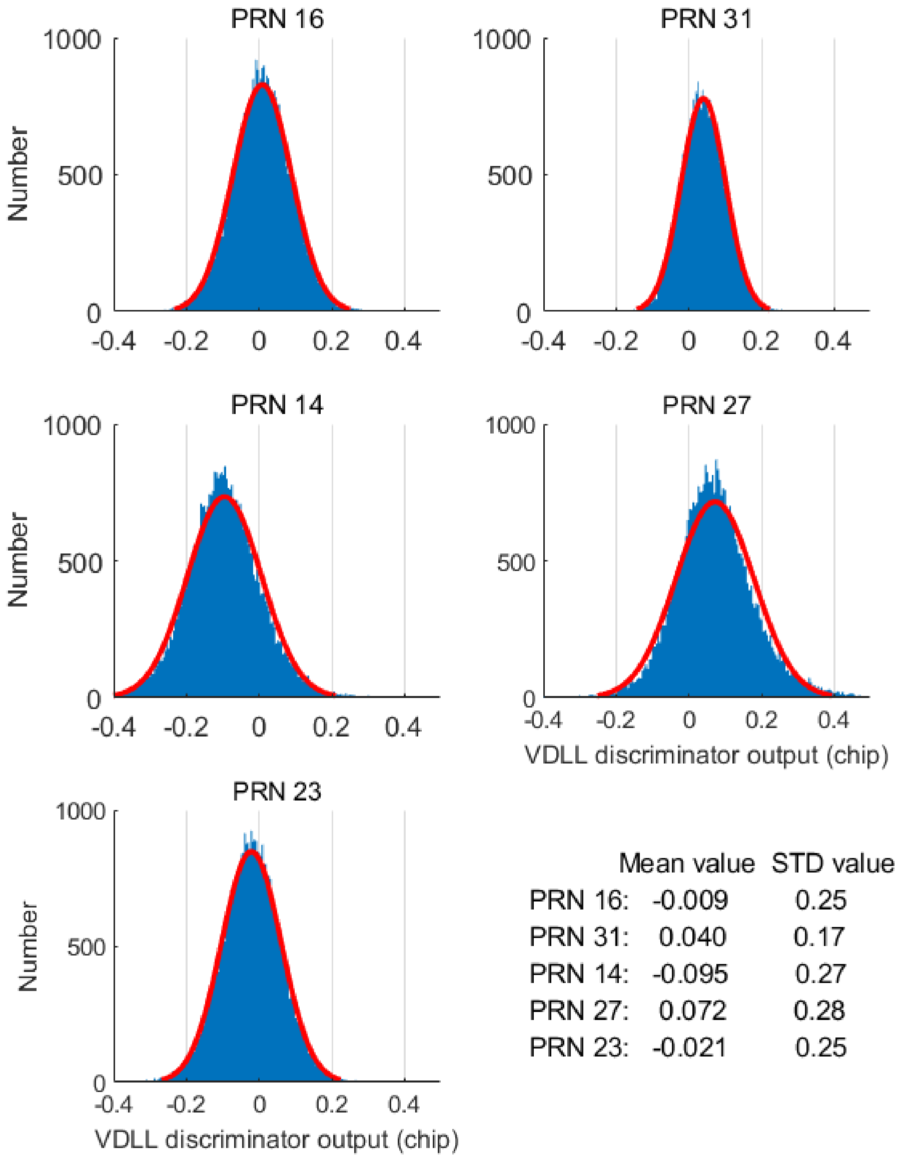

Fig. 4 GF results of the VDLL outputs for PRNs 14, 16, 23, 27, and 31. In general, the mean value of the code discriminator outputs in the VDLL approach are zero for LOS satellites

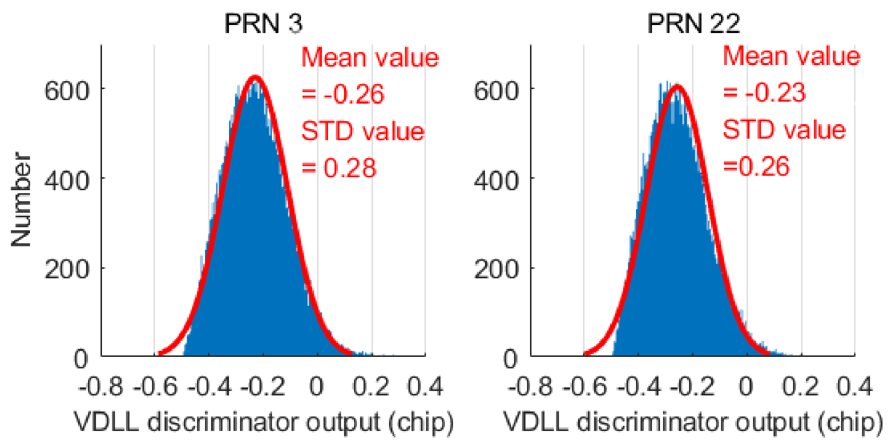

Fig. 5 GF results of the VDLL outputs for PRNs 3 and 22, which are NLOS satellites. Compared to the LOS satellites, the NLOS satellites have a larger code discriminator output offset in the VTL framework

As presented in (32), the detection threshold α and the number of code discriminator outputs being calculated N_{CE} affect the false alarm and detection probabilities. Once the model is fixed, the value of β is determined. Receiver operating characteristic (ROC) curves are usually used to present the relationship between the detection probability and false alarm probability (Radin et al. 2015). Fig. 6 presents the ROC curves for different values of β and N_{CE}. The parameter β is set to 1/4 to explore the influence of N_{CE} on the detection probability. For the same false alarm rate, the larger the value of N_{CE} is, the higher the detection probability. Then, to assess the influence of β on the detection probability, N_{CE} is set to 200. According to the curves presented in the bottom panel in Fig. 6, a larger β contributes to a better detection performance.

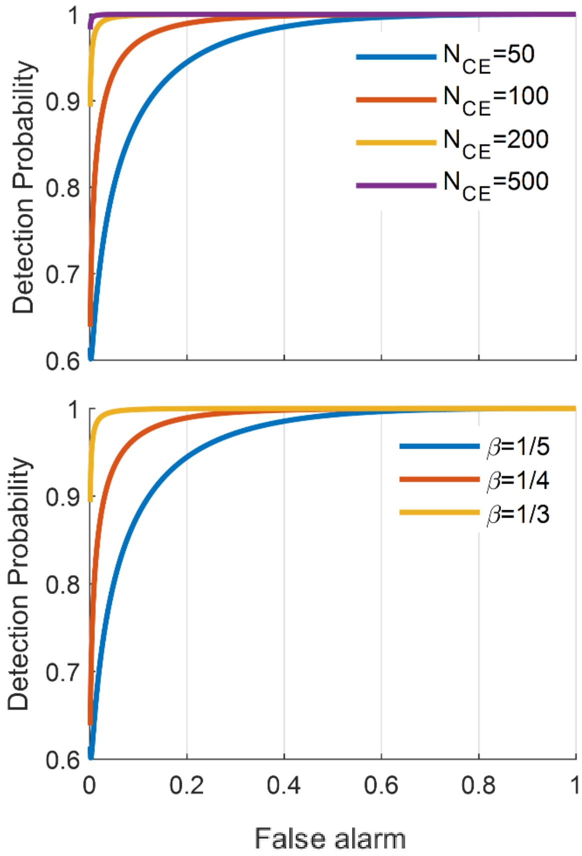

Fig. 6 Receiver operating characteristic (ROC) curves for different values of N_{CE} with fixed $\beta = 1/4$ (top) and for different values of β with fixed $N_{CE} = 200$ (bottom)

With the above analysis, here, the window sizes N_{CE} and α are set to 500 and 0.1 chips, respectively. The probability threshold of NLOS detection is set to 50%, which approximately equals 0.1 chips. Fig. 7 presents the LOS probability of detection (top panel) and the average VDLL discriminator output values over 500 ms (bottom panel) for PRNs 16, 31, 14, 27, and 23. Among these satellites, PRN 14 has the lowest LOS probability of detection. The LOS probability of the detection results is consistent with the corresponding average values. For instance, PRN 14 has the largest offset of code discriminator outputs, indicating the lowest detection probability. Fig 8 presents the NLOS detection probability and average values of the code discriminator outputs over 500 ms for PRNs 3 and 22. Both satellites have a probability of NLOS occurrence exceeding 60% during most of the experiment. Compared with conventional binary NLOS detection, the proposed approach can provide a probability of NLOS occurrence. In addition, the magnitude of this probability indicates the magnitude of the additional code delay of the NLOS signal. In other words, the NLOS probability is highly correlated with the additional NLOS code delay. For instance, in this experiment, PRN 22 has a larger additional code delay than PRN 3 in the first 30 seconds.

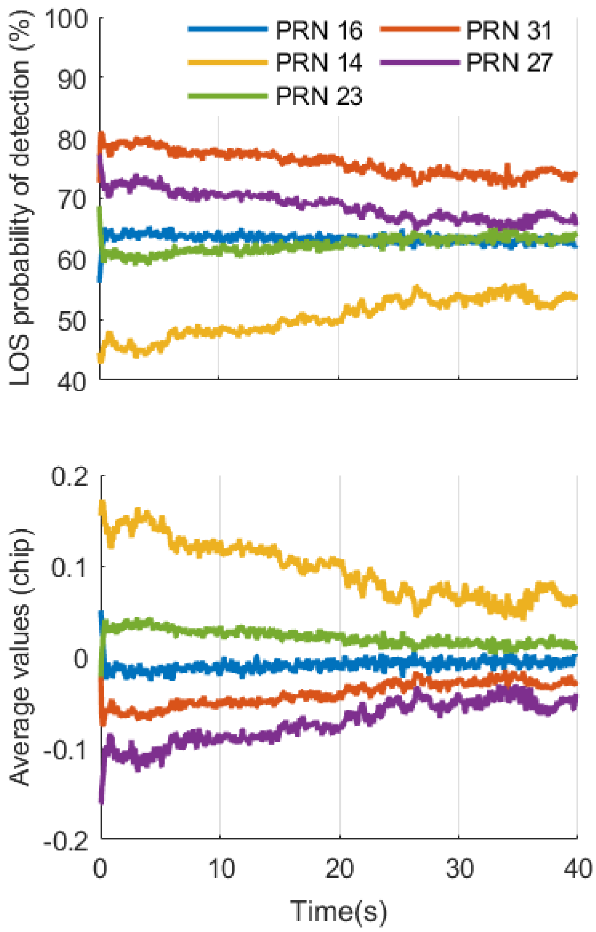

Fig. 7 LOS detection probability (top) and average values of VDLL discriminator output over 500 ms (bottom) for PRNs 16, 31, 14, 27, and 23

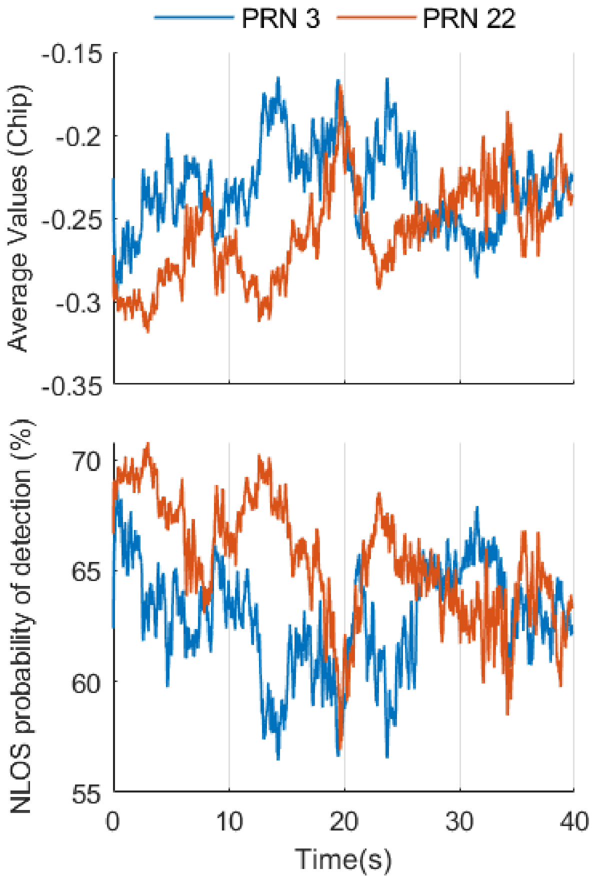

Fig. 8 Average values of the VDLL discriminator output (top) and NLOS detection probability (bottom) for PRNs 3 and 22

Fig. 9 presents the horizontal errors. The Standard VTL line indicates the result of the standard VTL method without considering NLOS reception. The line labelled "VTL with multicorrelator" represents the method of VTL-based NLOS detection and correction with multicorrelators proposed in Xu et al. (2020). In the VTL method with multicorrelators, the mean value of multiple correlator peaks is considered to be the additional code delay of the NLOS signal, which is then compensated for the pseudorange error measurements before feeding the measurements to the Kalman filter. The line labelled "VTL with an augmented state vector" signifies the result of the proposed approach. The statistical results of the positioning errors are listed in Table 2. Overall, the proposed approach slightly outperforms the other two methods in terms of both the mean and STD metrics. A closer look at Figs. 8 and 9 shows that when the

NLOS probability is higher, such as at periods of 0 to 8 s and 22 to 28 s, the improvement in the positioning performance is larger than that in other periods, indicating the effectiveness of the proposed approach. However, during the period of approximately 14 to 24 s, the proposed method has a larger positioning error than the VTL method with multicorrelators. Note that the NLOS probabilities of detection for both PRN 3 and PRN 22 are lower than 60% during this period, as shown in Fig. 8. A possible explanation is that the low probability of detection may degrade the performance of the proposed method.

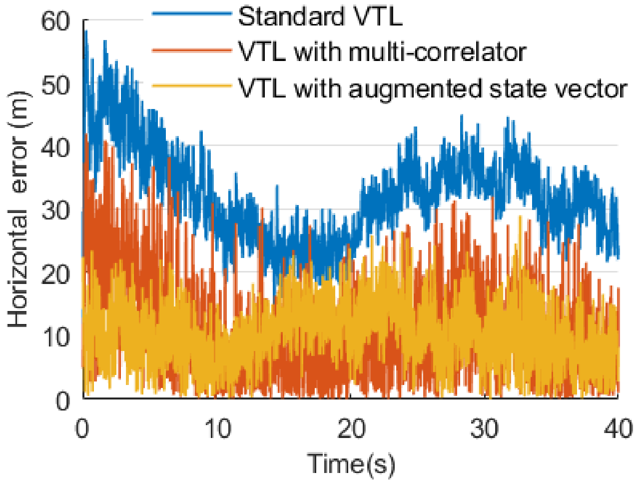

Fig. 9 Horizontal positioning errors using different algorithms

Table 2 Statistical results (mean and standard deviation (STD)) of the horizontal positioning errors for different algorithms (metres)

Algorithms	Standard VTL	VTL with multicorrelators	VTL with augmented state vector
Mean	32.6	10.6	9.8
STD	8.1	7.2	6.3

Dynamic Field Test

We also assess the proposed method using a dynamic IF dataset, which is the same as that used in our previous work (Xu et al. 2020). The route and street view are presented in Fig. 10. The antenna was carried by a pedestrian walking from Point 1 to Point 2; a more detailed description of the trajectory and the acquisition of the IF dataset can be found in Xu et al. (2020). The velocity in the east direction obtained using the VTL method with multicorrelators in Xu et al. (2020) is presented in Fig. 11, which is divided into four stages. 1) The pedestrian remained static at Point 1. The geometric distribution of the satellites in this period is presented in the middle panel of Fig. 10 (bottom left). All satellites tracked, i.e., PRNs 14, 22, 26, 31, and 32, are under the LOS condition without considering potential MP interference. 2) The pedestrian walked towards Point 2 (eastward) with a velocity of approximately 1 m/s. 3) The pedestrian stopped at Point 2 for a few seconds. The distribution of satellites at this stage is shown in the right panel of Fig. 10 (bottom right). We can see that PRN 31 is an NLOS satellite because its elevation angle is more than 15° lower than the building boundary at the same azimuth angle. According to the sky plot, PRN 22 is more likely to be diffracted, if not an NLOS satellite, because it is at the edge of the building boundary. 4) The pedestrian walked from Point 2 back to Point 1 along the same route.

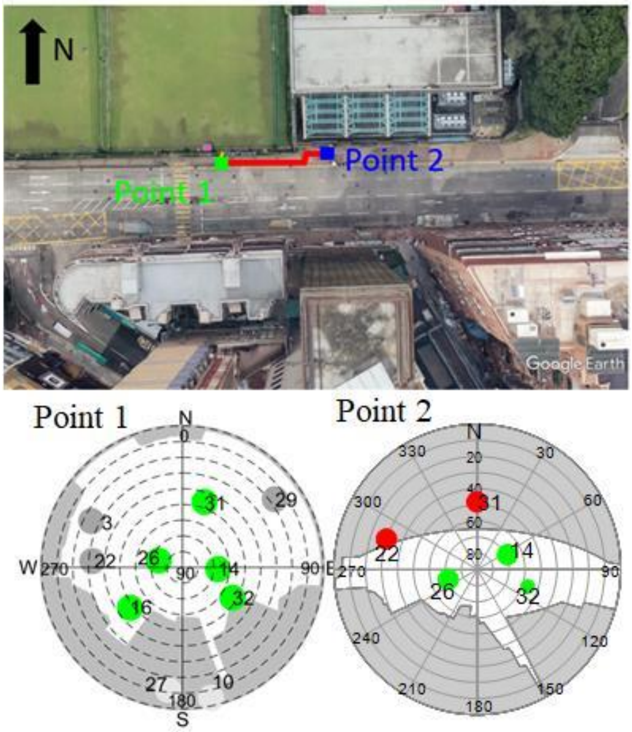

Fig. 10 Dynamic test trajectory (top) and sky plots at Points 1 (bottom left) and 2

(bottom right). The sky plot at Point 1 also gives the satellites (grey dots) that are present but cannot be tracked using the software receiver.

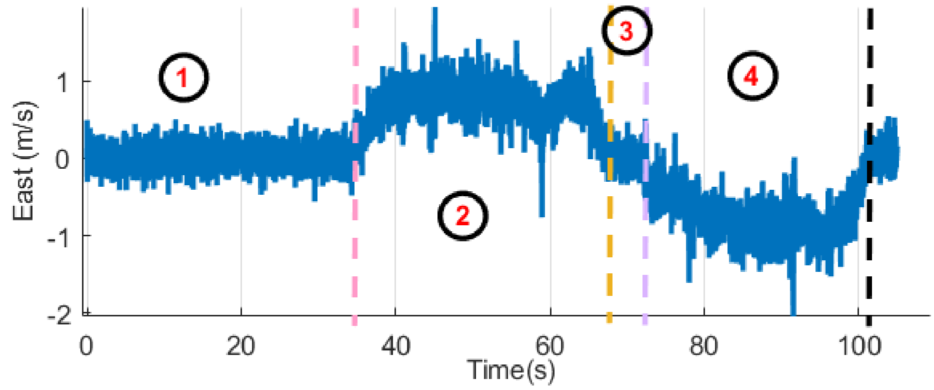

Fig. 11 Velocity in the east direction during the dynamic test, based on which the test period is divided into four stages for assessment

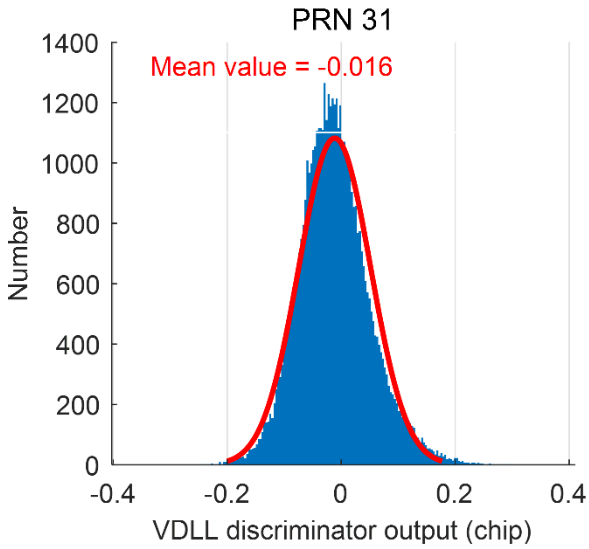

Fig. 12 GF results of the VDLL discriminator outputs for PRN 31 at Point 1

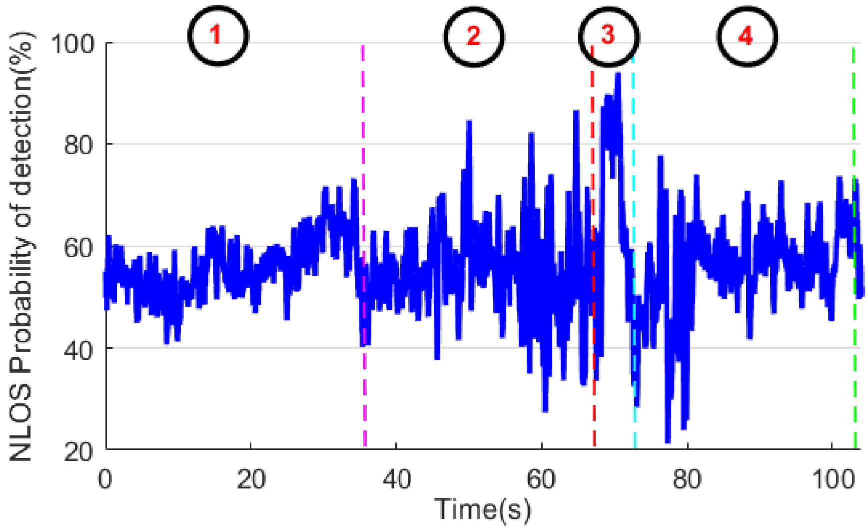

Fig. 13 NLOS probability for PRN 31. At stage 3, the NLOS detection probability exceeds 80% most of the time

In the first stage, PRN 31 is under the LOS condition, and the GF results for the VDLL discriminator output are presented in Fig. 12. Then, this model is employed to calculate the NLOS probability of PRN 31 at the following stages. The horizontal positioning errors for the three methods, i.e., the standard VTL method, the VTL method with multicorrelators, and the proposed method, are presented in Fig. 14, and the statistical analysis results are listed in Table 3. The ground truth trajectory was obtained based on the labelled features corresponding to the Google Earth with a timestamps record. At Point 2, the proposed VTL method with an augmented state vector outperforms the other two methods. Note that at this stage, the NLOS probability of PRN 31 exceeds 80%, as shown in Fig. 13. However, when the pedestrian was walking from 36 to 68 s, the VTL method with multicorrelators outperforms the proposed method, which may indicate that motion has an effect on NLOS detection. One of the reasons is that the proposed method is sensitive to the MP effect, as it detects NLOS signals based on code discriminator outputs. Therefore, MP errors caused by either user motion or satellite motion may produce a large code tracking error, which increases the false alarm probability of NLOS detection.

Table 4 lists the computational load analysis and comparison of the VTL method with multicorrelators with the VTL method with an augmented state vector. The software runs in MATLAB (Version 2018), and the computer is an ALIENWARE M15 laptop with an Intel Core I7 9750H CPU and 16 GB RAM. The code phase search range is -0.5 to 0.5 chips, and five satellites are processed. With the dataset of 104 seconds, there are $126\times5\times104\times1000$ correlators calculated in the VTL method with multicorrelators, while only $6\times5\times104\times1000$ correlators are calculated in the VTL method with an augmented state vector. As seen from Table 4, the running time for the correlation in the VTL method with multicorrelators is approximately 21 times that of the proposed method. Compared with the increased running time due to multicorrelators, the increased running time due to the addition of NLOS-induced pseudorange measurement errors to the standard state vector is much lower.

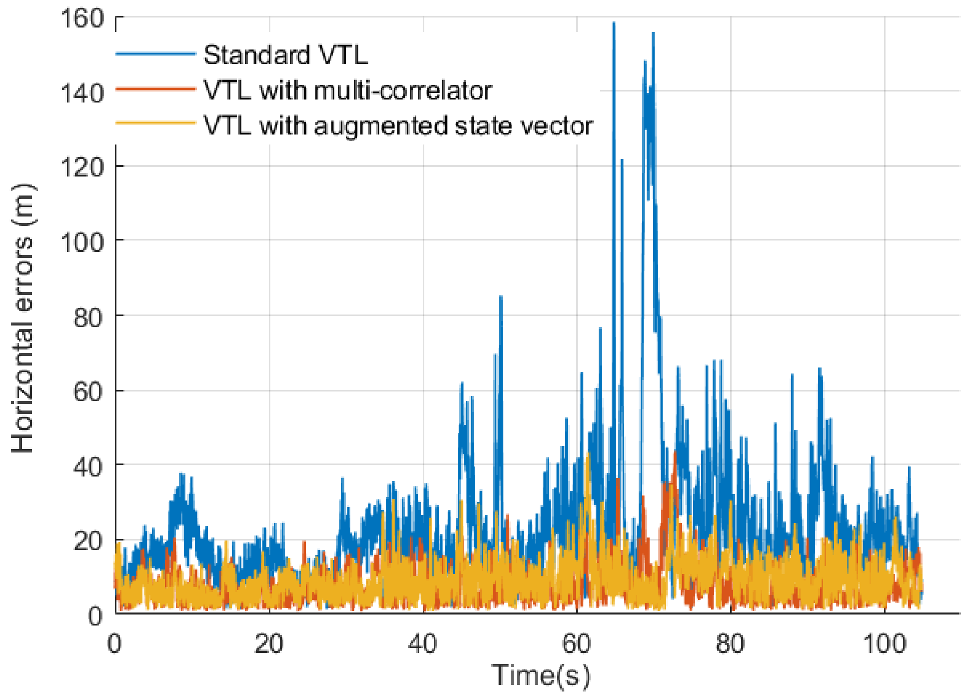

Fig. 14 Horizontal positioning errors for different algorithms in the dynamic test.

Table 3 Statistic values of the horizontal positioning errors (metres)

Time (s)	0-36		36-68		68-72		72-104	
Metrics	STD	Mean	STD	Mean	STD	Mean	STD	Mean
Standard	7.40	14.52	16.5	22.79	45.19	82.58	12.03	24.17

VTL								
VTL with multicorrelators	3.65	6.43	4.96	8.39	9.00	13.64	6.36	8.47
VTL with an augmented state vector	3.70	6.72	6.49	10.49	3.63	6.25	5.44	10.67

Table 4 Computational load and running time comparison

	Number of Correlators	Correlator Running Time (s)	State Vector Dimension	Measurement Vector Dimension	EKF Running Time (s)
VTL with multicorrelators	126×5×104000	3110.15	1×8	10×1	7.07
VTL with an augmented state vector	6×5×104000	147.91	1×10	10×1	7.59

Conclusions

We proposed a probabilistic approach to detect GNSS NLOS reception and correct its bias by augmenting the commonly used state vector. Two real-world datasets were tested, including both static and dynamic cases. The results demonstrate the feasibility of the proposed approach. Some concluding remarks can be made. On the one hand, the proposed approach generates the probability of NLOS detection. The higher the detection probability is, the greater the improvement in the positioning performance compared to other approaches. On the other hand, although an augmented state vector is introduced, the proposed method has a much lower computational load than the method that uses multicorrelators.

The following two directions are suggested for future work.

(1) The proposed approach can be extended to the application of MP detection and mitigation in the VTL framework. The principle behind this is that both MP- and NLOS-induced errors manifest themselves in the code discriminator outputs in the VTL (Hsu et al. 2015b).

(2) LiDAR is an active sensing technique for collecting ranging information of the surrounding environment, and the motion can be estimated through the collected point cloud (Hening et al. 2017). LiDAR can provide short-term accurate motion estimation to aid VTL, which would be beneficial for NLOS detection and correction.

References

Benson D (2007) Interference benefits of a vector delay lock loop (VDLL) GPS receiver. Proc. ION GNSS 2007, Institute of Navigation, Cambridge, MA, USA, April 23-25, 749-756

Breßler J, Reisdorf P, Obst M, Wanielik G (2016) GNSS positioning in non-line-of-sight context-a survey. In: 2016 IEEE 19th International Conference on Intelligent Transportation Systems (ITSC) Rio de Janeiro, Brazil, November 1-4, 1147 – 1154

Chen Y, Jiang C, Hyyppä J, Qiu S, Wang Z, Tian M, Li W, Puttonen E, Zhou H, Feng Z, Bo Y, Wen Z (2018) Feasibility study of ore classification using an active hyperspectral LiDAR. IEEE Geoscience and Remote Sensing Letters 15(11): 1785-1789

Copps EM, Geier GJ, Fidler WC, Grundy PA (1980) Optimal processing of GPS signals. Navigation 27(3):171-182

Hening S, Ippolito CA, Krishnakumar K.S, Stepanyan V, Teodorescu M (2017) 3D LiDAR SLAM integration with GPS/INS for UAVs in urban GPS-degraded environments. In: AIAA SciTech Forum, Grapevine, Texas, USA, January 9-13, pp 1-10

Hsu LT (2018) Analysis and modeling GPS NLOS effect in highly urbanized area. GPS Solutions 22:7. https://doi.org/10.1007/s10291-017-0667-9

Hsu LT, Gu Y, Kamijo S (2015a) NLOS correction/exclusion for GNSS measurement using RAIM and city building models. Sensors 15 (7): 17329-17349

Hsu LT, Jan SS, Groves PD, Kubo N (2015b) Multipath mitigation and NLOS detection using vector tracking in urban environments. GPS Solutions 19:249-262. https://doi.org/10.1007/s10291-014-0384-6

Jiang C, Chen S, Chen Y, Bo Y (2019) Research on a chip scale atomic clock aided vector tracking loop. IET Radar, Sonar & Navigation 13(7):1101-1106

Kaplan ED, Hegarty CJ (2005) Understanding GPS: principles and applications, 2nd edtion, Artech House, London

Lashley M, Bevly DM, Hung JY (2009) Performance analysis of vector tracking algorithms for weak GPS signals in high dynamics. IEEE Journal of Selected Topics in Signal Processing 3:661-673

Marais J, Meurie C, Attia D, Ruichek Y, Flancquart A (2014) Toward accurate localization in guided transport: combining gnss data and imaging information. Transportation Research Part C: Emerging Technologies, 43(pt.1), 188-197. https://doi.org/10.1016/j.trc.2013.11.008

Meguro JI, Murata T, Takiguchi JI, Amano Y, Hashizume T (2009). GPS multipath mitigation for urban area using omnidirectional infrared camera. IEEE Trans. Intell. Transp. Syst., 10(1): 22–30

Ng HF, Zhang G, Hsu LT (2020) A computation effective range-based 3D mapping aided GNSS with NLOS correction method. The Journal of Navigation, 1-21. https://doi.org/10.1017/S037346332000003X

Radin DS, Swaszek PF, Seals KC, Hartnett RJ (2015). GNSS spoof detection based on pseudoranges from multiple receivers. Proc. ION ITM, Dana Point, CA, USA, January 26-28, 657–671.

Spilker Jr. JJ (1996) Fundamentals of signal tracking theory. In: Parkinson B, Spilker Jr. JJ, Axelrad P, Enge P (eds) Global positioning system: Theory and applications, volume I, Charles Stark Draper Laboratory, Inc., Cambridge, Massachusetts, pp 245-327

Tsui JBY (2005) Fundamentals of Global Positioning System receivers: a software approach, 2nd edition. Wiley, New Jersey

Wang L, Groves P D, Ziebart M K. Smartphone Shadow Matching for Better Cross-street GNSS Positioning in Urban Environments [J]. Journal of Navigation, 2015, 68(3):411-433

Xu B, Hsu LT (2019a) An open source matlab code on GPS vector tracking based on software-defined receiver. GPS Solutions 23:46. https://doi.org/10.1007/s10291-019-0839-x

Xu B, Jia Q, Hsu LT (2020) Vector tracking loop-based GNSS NLOS detection and correction: Algorithm design and performance analysis. IEEE Transactions on Instrumentation and Measurement, 69(7): 4604-4619

Xu B, Jia Q, Luo Y, Hsu LT (2019b) Intelligent GPS L1 LOS/multipath/NLOS classifiers based on correlator-, RINEX- and NMEA-level measurements. Remote Sensing 11(16):1851.

Yozevitch R, Moshe BB, Weissman A (2016) A robust GNSS LOS/NLOS signal classifier. Navigation 63(4):429-442

Zhao S, Lu M, Feng Z (2011) Implementation and performance assessment of a vector tracking method based on a software GPS receiver. Journal of Navigation 64(S1):S151-S161.

Author Biographies

Changhui Jiang received a B.S. degree from Soochow University and a Ph.D. degree from Nanjing University of Science and Technology in 2014 and 2019, respectively. He studied as a visiting Ph.D. student at the Finnish Geospatial Research Institute (FGI) from 2017.12 to 2018.11 (sponsored by the China Scholarship Council (CSC)). He currently works as a Postdoctoral Fellow at The Hong Kong Polytechnic University. His research interests include hyperspectral LiDAR, GNSS signal processing, and multi-sensor integration.

Bing Xu is currently a Research Assistant Professor with the Interdisciplinary Division of Aeronautical and Aviation Engineering (AAE), The Hong Kong Polytechnic University (PolyU). He received his B.S. and Ph.D. degrees in network engineering and navigation guidance and control from Nanjing University of Science and Technology, China, in 2012 and 2018, respectively. From August 2018 to April 2020, he worked as a Postdoctoral Fellow with AAE, PolyU. His current research is in signal processing with applications to satellite navigation and wireless communications.

Li-Ta Hsu received B.S. and Ph.D. degrees in aeronautics and astronautics from National Cheng Kung University, Taiwan, in 2007 and 2013, respectively. He is currently an Assistant Professor with the Interdisciplinary Division of Aeronautical and Aviation Engineering, The Hong Kong Polytechnic University, before he served as a Postdoctoral Researcher in the Institute of Industrial Science at the University of Tokyo, Japan. In 2012, he was a visiting scholar at University College London, the U.K. His research interests include GNSS positioning in a challenging environment and localization for pedestrian, autonomous driving vehicles and unmanned aerial vehicles.